IEEE Photonics Journal
An IEEE Photonics Society Publication

Implant-Defined 3 × 3 In-Phase Coherently Coupled Vertical Cavity Surface Emitting Lasers Array

Volume 5, Number 6, December 2013

Ming-Ming Mao
Chen Xu
Yi-Yang Xie
Qiang Kan
Meng Xun
Kun Xu
Jun Wang
Hai-Qiang Ren
Hong-Da Chen

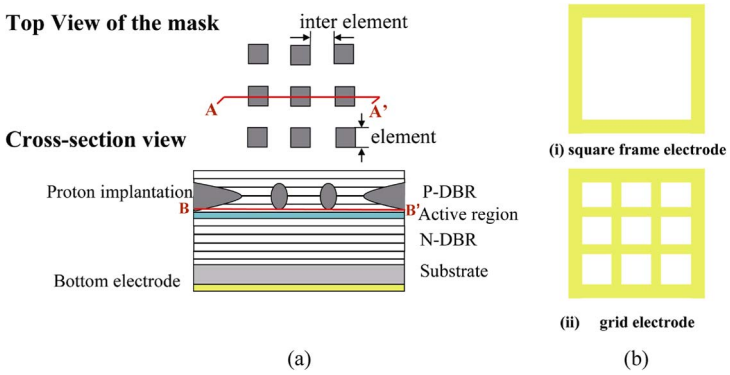

DOI: 10.1109/JPHOT.2013.2292351
1943-0655 © 2013 IEEE

Implant-Defined 3 × 3 In-Phase Coherently Coupled Vertical Cavity Surface Emitting Lasers Array

Ming-Ming Mao,[1] Chen Xu,[1] Yi-Yang Xie,[2] Qiang Kan,[2] Meng Xun,[1] Kun Xu,[1] Jun Wang,[1] Hai-Qiang Ren,[1] and Hong-Da Chen[2]

[1]Key Laboratory of Optoelectronics Technology, Ministry of Education, Beijing University of Technology, Beijing 100124, China
[2]State Key Laboratory of Integrated Optoelectronics, Institute of Semiconductor, Chinese Academy of Sciences, Beijing 100083, China

DOI: 10.1109/JPHOT.2013.2292351

Manuscript received October 24, 2013; revised November 3, 2013; accepted November 5, 2013. Date of publication November 21, 2013; date of current version December 4, 2013. This work was supported in part by the Nation Natural foundation of China under Grants 61076044, 61376049, 61204011, 61378058, and 61036009, by the National Basic Research Program of China under Grant 2010CB934104, by the Doctoral Fund of Ministry of Education of China under Grant 20121103110018, by the Natural Science Foundation of Beijing under Grant 4092007, and by the Beijing Committee of Education, China, under Grant PXM2013_014204_000029. Corresponding author: C. Xu (e-mail: xuchen58@bjut.edu.cn).

Abstract: Two-dimensional in-phase coherently coupled vertical cavity surface emitting laser (VCSEL) array with high beam quality was fabricated by proton implantation. Indium–tin–oxide (ITO) current spreading layer was employed to improve the uniformity of the injection current. This makes a coherent array to operate in in-phase mode even in a relatively larger scale. The appropriate thickness of ITO current spreading layer was obtained by experiment (80 nm). The procedure of proton implantation defined array is considerably simple and low cost. A 3 × 3 in-phase coherently coupled array with 2.4° (1.28 × D.L.) of lobe beamwidth was achieved. It sufficiently demonstrates the advantages of the high beam quality of the in-phase coherently coupled arrays. The output power of the array was up to 4.5 mw under pulse-wave condition.

Index Terms: Coherently coupled VCSEL array, in-phase, high beam quality.

1. Introduction

Array integration is a method often used to obtain a high laser power output. Compared with the traditional edge emitting lasers, the vertical cavity surface emitting lasers (VCSELs) get an increasing interest due to the obvious advantages in the realization of two-dimensional integration [1], [2]. However, it is desirable to use coherence light sources with higher brightness rather than those only with higher power in the application of imaging, optical interconnects, parallel optical signal process and communication [3], [4]. Therefore, the arrays operating in in-phase coherently coupled mode are preferred in order to get an on-axis angular narrow beam far field, even a near-diffraction-limited [5], [6] beam quality so that the optical energy can be concentrated in the central lobe.

To achieve effective coherently coupled among the VCSELs in an array, a variety of methods have been tried. The first report of coherently coupled VCSEL array came from Yoo *et al.* [7] through air gap between VCSELs. After that, reflectivity-modulated VCSEL arrays [8] were proposed by etching features in the DBR mirror. However, the out-of phase array modes were normally obtained by these methods. Photonic crystal architecture and proton implantation can be combined [9] to make the

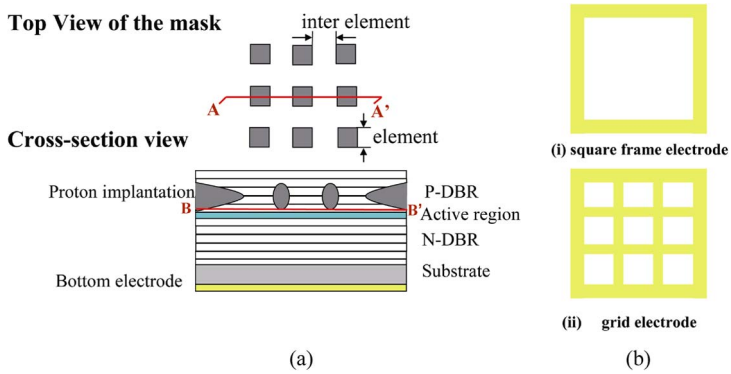

Fig. 1. (a) Schematic cross-section view of the array and the top view of the mask. (b) Two kinds of electrode: the square frame electrode and the grid electrode.

elements in the array coherently couple in phase with a small scale (2 $\times$ 2). The anti-guide effect can be generated by the carrier induced index depression and the thermal lens for this proton implantation array, with an approximate index step of $3 \times 10^{-3} \sim 4 \times 10^{-3}$ to keep a steady coupling among element. However, when the scale is as large as 3 $\times$ 3, or higher, the array suffers from the non-uniformity of injection current. The injection currents are insufficient in those elements far away from the electrodes, which would delay in their lasing, even affect the coupling between the array elements seriously. The patterning metal grid electrode [10], [11] can improve the uniformity of the injection current. Nevertheless, the out-of-phase modes or other adjacent modes will be in dominant due to the absorption loss introduced by the metal electrode in the inter element region. In this case, the far field shows twin-lobed on-axis null, inconvenient to fiber collimation and focusing. On the other hand, cavity induced anti-guide structure array has a very strong mode selection capability due to the inherent leak wave coupling mechanism. So the array can still work in an in-phase mode even if the metal grid is applied to deal with the uniformity of injection current. 4 $\times$ 4 and 5 $\times$ 5 in-phase coupled arrays have been achieved by Delai Zhou [12] and Lin Bao [13], respectively. However, secondary epitaxial growth processes were used to get their cavity induced anti-guide structure, and the performance of the array was very sensitive to the dimension of inter element region, leading an increasing of fabrication complexity and cost. In this paper, two dimensional (2-D) coherently coupled arrays of vertical cavity surface emitting lasers (VCSELs) were fabricated by proton implantation. The procedure for the array is considerably simple and the cost is low. The appropriate thickness of ITO current spreading layer was employed on the p-type top DBR to improving the uniformity of the injection current. A 3 $\times$ 3 in-phase coherently coupled array was achieved with an output power of 0.36 mw and 4.5 mw under continuous wave and under pulse, respectively at room temperature. The far field divergence angle is 2.4°, up to 1.28 $\times$ D.L.

2. Experimental Details

The VCSEL epitaxial structure with 850-nm emission wavelength was grown on an n-GaAs substrate. The quantum well is GaAs and the barrier layer is $Al_{0.3}Ga_{0.7}As$. (This article is focused on the coherently coupled array, so we employed the conventional quantum well. As to the 850 nm emitting VCSELs, the AlInGaAs, InGaAsP strain quantum well and narrow InGaAs quantum well can improve the differential gain in the active regions, thus resulted in both high speed and high temperature characteristics.) The material contains 22.5-pairs of p-type top DBR and 34.5-pairs of n-type bottom DBR, consisting of alternating $Al_{0.9}Ga_{0.1}As/Al_{0.12}Ga_{0.88}As$ layers. The DBR doping concentration is $3.5 \times 10^{18}/cm^3$ and has a $1.9 \times 10^{19}/cm^3$ concentration in the top ohmic contact layer. All the array element dimensions are 6 μm $\times$ 6 μm. The inter element region was chosen to 4 μm to allowing for a single lasing fringe between array elements. Proton implantation was used to define the apertures of the array. A schematic cross-section view of the array and the top view of the mask are shown in Fig. 1. A thick silicon dioxide mask was formed by PECVD and ICP

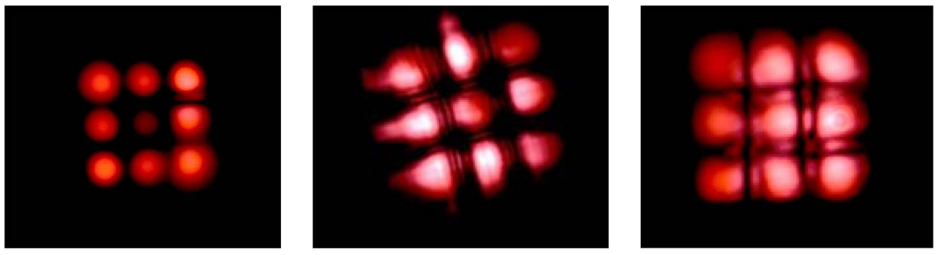

Fig. 2. Lasing near field images of the three kinds of structure. (a) Structure 1: square frame electrode and without ITO current spreading layer at the injection current of 15.2 mA; (b) structure 2: grid electrode and without ITO current spreading layer at the injection current of 16.5 mA; (c) structure 3: square frame electrode and with 80 nm ITO current spreading layer on the p-type top DBR at the injection current of 14.3 mA.

etching. Then, the proton implantation was performed at a dose and energy of $1 \times 10^{15}/\text{cm}^2$ and 315 kev, respectively. The array scale is 3×3. As shown in Fig. 1, two kinds of metal electrode were prepared, the square frame electrode and the grid electrode. Three kinds of structure were fabricated respectively, namely structure 1: square frame electrode and without ITO current spreading layer; structure 2: metal grid electrode and without ITO current spreading layer; structure 3: square frame electrode and with 80 nm ITO current spreading layer on the p-type top DBR.

3. Results

Fig. 2 is the near field profile of the three structures aforementioned. From Fig. 2(a), we can find that the light intensity of the central element is very weak and the coupling among elements is insufficient (without characteristic fringes between elements). This is caused by non-uniformity of the injection current due to square frame electrode and lack of ITO current spreading layer in structure 1. The injection current level is abnormally low in the elements away from the electrodes. On the contrary, the grid electrode used in structure 2 [Fig. 2(b)] can offer the equal current to all elements, insuring them lasing at the same time. However, because of optical absorption by the metal in the inter element region, the fundament in-phase mode (only one fringe between the elements) was depressed, and two fringes appeared instead between the elements, indicating an out-of-phase coupling mode. Since the ITO current spreading layer was introduced in the structure 3, the uniformity of injection current was greatly improved though the square frame electrode was used. Moreover, there is only one fringe in the inter element region [Fig. 2(c)], a typically features of the fundamental in-phase mode which can also be confirmed in the far field distribution shown in Fig. 6.

To describe the improvement of the uniformity of the injection current by ITO current spreading layer, COMSOL was used to simulate the current distribution of structure 1 and structure 3. We consider a position above the active region and below the peak zone of the proton implantation (e.g.: Fig. 1 B-B′ position). Herein, the injection current flows from the beam aperture into the active region and the bottom electrode is far from it. Consequently, the current is almost perpendicular to the B-B′ plane. Thereby, the B-B′ plane can be taken as an equipotential plane [14] and be equivalent to a metal electrode. Each P-type DBR layer was treated as a homogeneous resistance. By applying a voltage between the square frame electrode and the equivalent electrode, the current distribution in the B-B′ plane can be simulated, as shown in Fig. 3. It can be seen that the array of structure 1 suffers from the non-uniformity of injection current, especially in the central element. This would affect the coupling between the array elements seriously. The calculated current density distribution of structures 1 and 3 in the B-B′ plane along the A-A′ direction (see Fig. 1) is illustrated in Fig. 4, where the sheet resistance of the ITO is taken as 30 ohm, a measured value. It can be seen that the difference of current density between the central element and the elements close to the electrode was significantly reduced since the 80 nm ITO current spreading layer was introduced, which effectively supported the coupling among elements. The uniformity of current distribution will be further improved

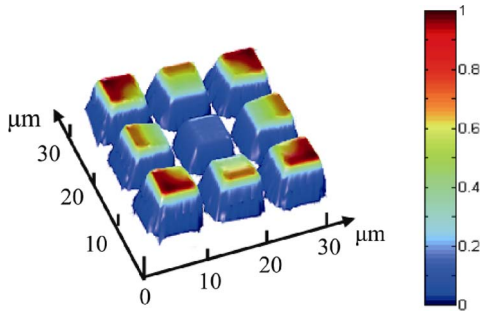

Fig. 3. Current distribution of the structure 1 in the B-B′ plane simulated by COMSOL. The color bar is the normalized current intensity.

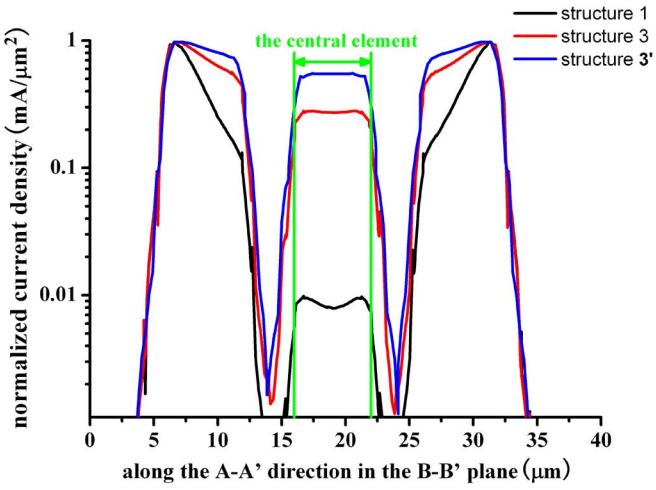

Fig. 4. Calculate current density distribution of structures 1 and 3 in the B-B′ plane along the A-A′ direction. The sheet resistance of the ITO is taken as 30 ohm and each P-type DBR layer was treated as a homogeneous resistance.

if the sheet resistance of current spreading layer can be reduced to 10 ohm (see the curve of structure 3′ shown in the Fig. 4). As can be seen in the inset of Fig. 6, the threshold currents of structure 2 and structure 3 are 9.2 mA and 10.1 mA, respectively, implying the sufficient current spreading in structure 3 thanks to the ITO layer.

The near field and far field distribution can be utilized to judge whether the output status is in-phase, showing an on-axis maximum in the far field, or out-of-phase, showing twin-lobed on-axis null. According to the near field experiment results shown in Fig. 2, only one fringe appeared in the inter element region of structure 3, indicating a phase difference of 0 or 2π between the adjacent element. Similarly, there were two fringes in the inter element region of structure 2, indicating a phase difference of π or 3π between the adjacent elements [15]. FDTD-solution was used to simulate the two situations. The distribution of the far field was simulated after setting the phase of each element. The result is shown in Fig. 5. The circles represent emission degree from the normal of laser facet. When the phase difference between the adjacent elements is 0 or 2π, the far field patterns demonstrate an on-axis maximum [Fig. 5(a)]. When the phase difference between the adjacent elements is π or 3π, the far field patterns demonstrate an on-axis null [Fig. 5(b)]. This simulation result agrees well with the experiment result.

The far field distributions in one dimensional scanning of structure 2 and structure 3 are shown in Fig. 6. It can be seen that the far field distribution of structure 3 and structure 2 are an on-axis maximum and an on-axis null, respectively, corresponding to the in-phase and out-of-phase mode,

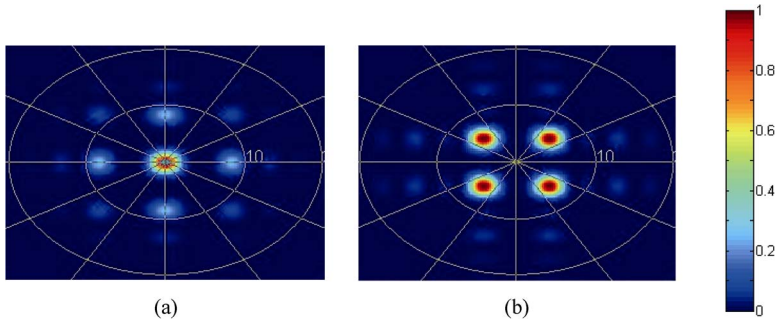

Fig. 5. Simulated far field (a) an in phase on-axis maximum far field and (b) an out of phase on-axis null far field. The simulated distributions of the far field according to the near field experiment results shown in Fig. 2(b) and (c). The circle represents emission degree from the normal of the laser facet and the color bar is the normalized intensity.

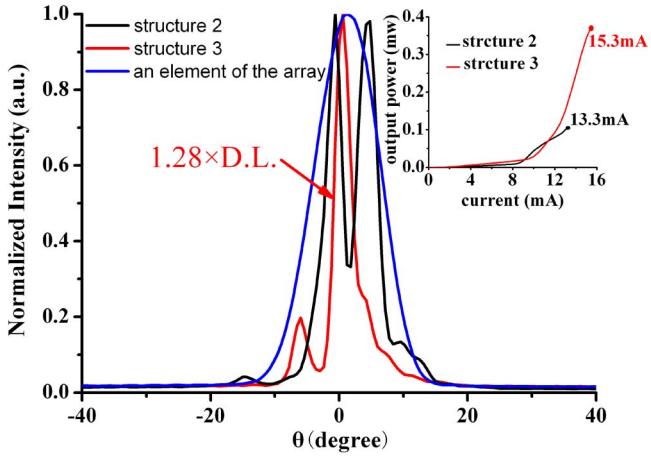

Fig. 6. Far field distributions in one dimensional cross section scanning of structure 2 and structure 3 at 13.3 mA and 15.3 mA under CW at room temprature, respectively. The far-field lobe Full Width at Half Maximum of structure 3 is 2.4° (1.28 × D.L.). The blue line is the far field distributions of an element of the array. Inset: the P-I curve of structure 2 and structure 3 under CW at roomtemprature, the threshold currents are about 9.2 mA and 10.1 mA, respectively.

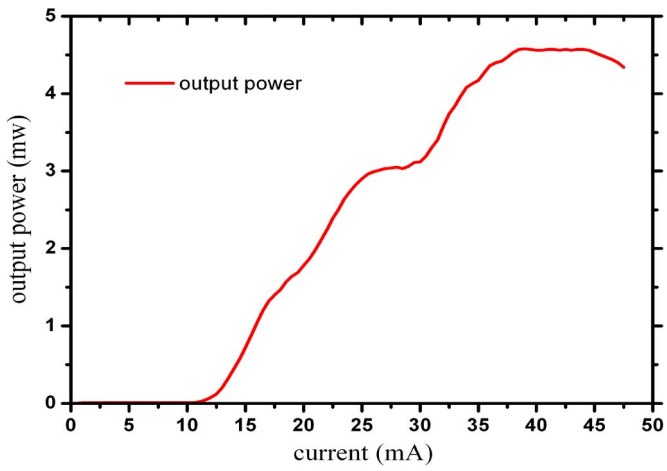

Fig. 7. P-I curve of structure 3 under pulse wave condition with a duty cycle 0.2% and pulse frequency 100 Hz, respectively.

respectively. It should be noted that the far field divergence angle of structure 3 is only 2.4°, up to 1.28 × D.L. and is far less than that of an element of the array (10°). This indicates the benefit of a coherently coupled array operating in in-phase mode in order to acquire a smaller divergence angle, even to the diffraction limit. In this way, the beam energy can be concentrated to obtain a high brightness light source. Fig. 7 is the P-I curve of structure 3 under pulse-wave condition with a duty cycle 0.2% and pulse frequency 100 Hz, respectively. The output power of the array was 4.5 mw.

4. Conclusion

3 × 3 in-phase coherently coupled arrays were achieved by improving the uniformity of the injection current via ITO current spreading layer. The far field divergence angle is 2.4°, up to 1.28 × D.L. It sufficiently demonstrates the advantages of the high beam quality of the in-phase coherently coupled arrays. The output power of the array was up to 4.5 mw under pulse-wave condition with a duty cycle 0.2% and pulse frequency 100 Hz, respectively. The metal grid electrode can make the injection current more uniform and can suppress the non-resonant mode in the anti-guide array structure. However, it can get the out of phase output mode almost time. The procedure of proton implantation is also considerably simple and can be used as alternative to other array implementations due to the low cost.

References

[1] H. Naito, M. Miyamoto, Y. Aoki, A. Higuchi, K. Torii, T. Nagakura, T. Morita, J. Maeda, H. Miyajima, and H. Yoshida, "Development of a high power vertical-cavity surface-emitting laser array with ion-implanted current apertures," in *Proc. SPIE*, 2013, vol. 8639, pp. 86390N-1–86390N-8.
[2] M. Grabherr, M. Miller, R. Jager, R. Michalzik, U. Martin, H. J. Unold, and K. J. Ebeling, "High-power VCSEL's: Single devices and densely packed 2-D-arrays," *IEEE J. Sel. Topics Quantum Electron.*, vol. 5, no. 3, pp. 495–502, May/Jun. 1999.
[3] D. F. Siriani and K. D. Choquette, "Electronically controlled two-dimensional steering of in-phase coherently coupled vertical-cavity laser arrays," *IEEE Photon. Technol. Lett.*, vol. 23, no. 3, pp. 167–169, Feb. 2011.
[4] J. S. Harris, T. O'Sullivan, T. Sarmiento, M. M. Lee, and S. Vo, "Emerging applications for vertical cavity surface emitting lasers," *Semicond. Sci. Technol.*, vol. 26, no. 1, pp. 0140101-1–0140101-11, Jan. 2011.
[5] D. Botez, L. Mawst, P. Hayashida, G. Peterson, and T. J. Roth, "High-power, diffraction-limited-beam operation from phase-locked diode-laser arrays of closely spaced leaky wave-guides (antiguides)," *Appl. Phys. Lett.*, vol. 53, no. 6, pp. 464–466, Aug. 1988.
[6] D. Botez, "Array-mode far-field patterns for phase-locked diode-laser arrays - coupled-mode theory versus simple diffraction theory," *IEEE J. Quantum Electron.*, vol. QE-21, no. 11, pp. 1752–1755, Nov. 1985.
[7] H. J. Yoo, A. Scherer, J. P. Harbison, L. T. Florez, E. G. Paek, B. P. Vandergaag, J. R. Hayes, A. Vonlehmen, E. Kapon, and Y. S. Kwon, "Fabrication of a 2-dimensional phased-array of vertical-cavity surface-emitting lasers," *Appl. Phys. Lett.*, vol. 56, no. 13, pp. 1198–1200, Mar. 1990.
[8] P. L. Gourley, M. E. Warren, G. R. Hadley, G. A. Vawter, T. M. Brennan, and B. E. Hammons, "Coherent beams from high-efficiency 2-dimensional surface-emitting semiconductor-laser arrays," *Appl. Phys. Lett.*, vol. 58, no. 9, pp. 890–892, Mar. 1991.
[9] J. J. Raftery, A. C. Lehman, A. J. Danner, P. O. Leisher, A. V. Giannopoulos, and K. D. Choquette, "In-phase evanescent coupling of two-dimensional arrays of defect cavities in photonic crystal vertical cavity surface emitting lasers," *Appl. Phys. Lett.*, vol. 89, no. 8, pp. 081119-1–081119-3, Aug. 2006.
[10] M. Orenstein, E. Kapon, N. G. Stoffel, J. P. Harbison, L. T. Florez, and J. Wullert, "2-dimensional phase-locked arrays of vertical-cavity semiconductor-lasers by mirror reflectivity modulation," *Appl. Phys. Lett.*, vol. 58, no. 8, pp. 804–806, Feb. 1991.
[11] T. Fishman, E. Kapon, H. Pier, and A. Hardy, "Modal expansion analysis of strained photonic lattices based on vertical cavity surface emitting laser arrays," *Appl. Phys. Lett.*, vol. 74, no. 24, pp. 3595–3597, Jun. 1999.
[12] D. Zhou and L. J. Mawst, "Two-dimensional phase-locked antiguided vertical-cavity surface-emitting laser arrays," *Appl. Phys. Lett.*, vol. 77, no. 15, pp. 2307–2309, Oct. 2000.
[13] L. Bao, N. H. Kim, L. J. Mawst, N. N. Elkin, V. N. Troshchieva, D. V. Vysotsky, and A. P. Napartovich, "Modeling, fabrication, and characterization of large aperture two-dimensional antiguided vertical-cavity surface-emitting laser arrays," *IEEE J. Sel. Topics Quantum Electron.*, vol. 11, no. 5, pp. 968–981, Sep./Oct. 2005.
[14] R. P. Sarzala, W. Nakwaski, and M. Osinski, "Effects of carrier diffusion on thermal properties of proton-implanted top-surface-emitting lasers," in *Proc. SPIE*, 1995, vol. 2399, pp. 583–604.
[15] G. R. Hadley, "Index-guided arrays with a large index step," *Opt. Lett.*, vol. 14, no. 6, pp. 308–310, Mar. 1989.